

Q^2 -dependence of backward pion multiplicity in neutrino-nucleus interactions

O. Benhar¹, S. Fantoni², G.I. Lykasov^{3†}, U. Sukhatme⁴

¹ *INFN, Sezione Roma 1, I-00185 Rome, Italy*

² *International School for Advanced Studies (SISSA), I-34014 Trieste, Italy*

³ *Joint Institute for Nuclear Research, Dubna 141980, Moscow Region, Russia*

⁴ *Dept. of Physics, University of Illinois, Chicago, IL 60607, USA*

(November 7, 2018)

Abstract

The production of pions emitted backward in inelastic neutrino-nucleus interactions is analyzed within the impulse approximation in the framework of the dual parton model. We focus on the Q^2 -dependence of the multiplicity of negative pions, normalized to the total cross section of the reaction $\nu + A \rightarrow \mu + X$. The inclusion of planar (one-Reggeon exchange) and cylindrical (one-Pomeron exchange) graphs leads to a multiplicity that decreases as Q^2 increases, in agreement with recent measurements carried out at CERN by the NOMAD collaboration. A realistic treatment of the high momentum tail of the nucleon distribution in a nucleus also allows for a satisfactory description of the semi-inclusive spectrum of backward pions.

PACS numbers: 13.60Le, 25.30Fj, 25.30Rw

Typeset using REVTeX

Over the past several years, backward hadron production in inelastic lepton-nucleus scattering has been extensively investigated, both experimentally [1–3] and theoretically [4–8], with the aim of pinning down the dominant reaction mechanism and extracting information on the underlying dynamics.

The analysis carried out on refs. [6,7] focused on nuclear effects in $e + A \rightarrow e' + p + X$ reaction, while in ref. [8], hereafter referred to as I, we studied the spectrum of pions emitted in the process $\nu + A \rightarrow \mu + \pi + X$. The results in I show that the main contribution to this spectrum comes from scattering off nucleons carrying high momentum. The calculations were performed within the impulse approximation (IA) scheme, using the Quark Gluon String Model (QGSM) [9,10] to describe the interaction vertex. This model is similar to the Dual Parton Model (DPM) developed in refs. [11,12], in that both approaches are aimed at implementing the dual topological unitarization scheme. The relativistic invariant semi-inclusive spectrum of pions emitted strictly backward was obtained including only the cylindrical (i.e. one-Pomeron exchange) graph, while the contribution of the planar (i.e. one-Reggeon exchange) diagram was neglected.

In this paper we continue the investigation of semi-inclusive pion production, started in I. We extend our analysis to pions emitted in the whole backward hemisphere, with respect to the direction of the incoming beam, and use QGSM to consistently include both the cylindrical and planar graphs in the calculation of the spectrum integrated over the transverse pion momentum. Our results are compared to the new data from the NOMAD collaboration [3], which measured the spectrum of π emitted in the backward hemisphere in the reaction $\nu + C \rightarrow \mu + \pi + X$ and the Q^2 -dependence of the pion multiplicity, $\langle n_\pi \rangle$, normalized to the total cross section of the reaction $\nu + C \rightarrow \mu + X$.

Our study focuses on the kinematical region of large pion momentum ($p_\pi > 0.3 \text{ GeV}/c$), where the effects of final state interactions (FSI) leading to pion absorption associated with production of baryon resonances are expected to be small [13,14] and the IA can be safely used.

The relativistic invariant semi-inclusive spectrum of pions produced in the process $\ell +$

$A \rightarrow \ell' + \pi + X$, in which the incoming lepton is scattered with energy E' into the solid angle $d\Omega$, is defined as

$$\rho_{\ell A \rightarrow \ell' \pi X} \equiv E_\pi \frac{d\sigma}{d^3 p_\pi d\Omega dE'} , \quad (1)$$

where E_π and \mathbf{p}_π are the total energy and three momentum of the produced pion, respectively. Within the framework of IA the quantity appearing on the right hand side of the above equation can be rewritten in convolution form, in terms of the semi-inclusive spectra of pions produced in lepton-proton and lepton-neutron processes $\rho_{\ell p \rightarrow \ell' \pi X}$ and $\rho_{\ell n \rightarrow \ell' \pi X}$, according to (see, e.g., refs. [6,8,15])

$$\begin{aligned} \rho_{\ell A \rightarrow \ell' \pi X}(x, Q^2; z, p_{\pi t}) &= \int_{x, z \leq y} dy d^2 k_t f_A(y, k_t) \left[\frac{Z}{A} \rho_{\ell p \rightarrow \ell' \pi X} \left(\frac{x}{y}, Q^2; \frac{z}{y}, p_{\pi t} - \frac{z}{y} k_t \right) \right. \\ &\quad \left. + \frac{N}{A} \rho_{\ell n \rightarrow \ell' \pi X} \left(\frac{x}{y}, Q^2; \frac{z}{y}, p_{\pi t} - \frac{z}{y} k_t \right) \right] , \end{aligned} \quad (2)$$

where Z and N are the number of protons and neutrons, $A = Z + N$ and $Q^2 = -q^2$, q being the four-momentum transferred by the lepton. The relativistic invariant variables x and z are defined as [2,3]

$$x = \frac{M_A}{m} \frac{Q^2}{2(P_A \cdot p_\nu)} , \quad z = \frac{M_A}{m} \frac{(p_\pi \cdot p_\nu)}{(P_A \cdot p_\nu)} , \quad (3)$$

where P_A and p_ν are the four-momenta of the nucleus and the initial neutrino, respectively, and M_A and m are the nucleus and nucleon masses. The above variables are best suited to analyze the data of ref. [3], in which the backward direction is defined with respect to the beam direction. Note that they do not coincide with x and z employed in I, whose definition can be recovered by replacing the four-momentum of the incoming neutrino, p_ν , with the four momentum transfer q in eq.(3).

The nucleon distribution function $f_A(y, k_t)$ can be written [6]

$$f_A(y, k_t) = \int dk_0 dk_z S(k) y \delta \left(y - \frac{M_A}{m} \frac{(k \cdot p_\nu)}{(P_A \cdot p_\nu)} \right) \quad (4)$$

where $S(k)$ is the relativistic invariant function describing the nuclear vertex with an outgoing virtual nucleon. The function $f_A(y)$ resulting from the transverse momentum integration

of $f_A(y, k_t)$ can be obtained by approximating $S(k)$ with the nonrelativistic spectral function $P(\mathbf{k}, E)$ yielding the probability of finding a nucleon with momentum \mathbf{k} and removal energy $E = m - k_0$ in the target nucleus [16]. However, due to the limited range of momentum and removal energy covered by nonrelativistic calculations of $P(\mathbf{k}, E)$ (typically $|\mathbf{k}| < k_{max} \sim 0.7 - 0.8$ GeV/c and $(m - k_0) < 0.6$ GeV. (see, e.g., ref. [16]), this procedure can only be used in the region $y < y_0 \sim 1.7 - 1.85$. An alternative approach to obtain $f_A(y)$ at larger y , based on the calculation of the overlap of the relativistic invariant phase-space available to quarks belonging to strongly correlated nucleons, has been proposed in ref. [6]. A similar procedure has been also used in ref. [13] to obtain the quark distribution in deuteron at large y .

The analysis of backward pion production requires the full nucleon distribution function given by eq.(4). We assume that it can be written in the factorized form

$$f_A(y, k_t) = f_A(y)g_A(k_t) , \quad (5)$$

with the function g_A chosen of the Gaussian form

$$g_A(k_t) = \frac{1}{\pi \langle k_t^2 \rangle} e^{-k_t^2 / \langle k_t^2 \rangle} , \quad (6)$$

where $\langle k_t^2 \rangle$ is the average value of the squared nucleon transverse momentum.

The second ingredient entering the calculation of the spectrum of eq.(2) is the elementary semi-inclusive spectrum. It can be calculated within the QGSM, based on the $1/N$ expansion, N being the number of flavors or colors, developed in [10]. According to ref. [9], the elementary production process can be described in terms of planar and cylindrical graphs in the s -channel, as shown in fig. 1 for the case of neutrino interactions associated with the exchange of a W -boson. The planar graph of fig. 1 (a) describes neutrino scattering off a valence quark. According to [5,8] its contribution to the process $\nu + N \rightarrow \mu + \pi + X$ reads

$$F_P^N(x_1, Q^2; z_1, p_{1t}) = z_1 \phi_1(x_1, Q^2) \left[\frac{1}{3} D_{uu \rightarrow \pi} \left(\frac{z_1}{1-x_1}, p_{1t} \right) + \frac{2}{3} D_{ud \rightarrow \pi} \left(\frac{z_1}{1-x_1}, p_{1t} \right) \right] , \quad (7)$$

with

$$\phi_1(x_1, Q^2) = \frac{G^2 m E}{\pi} \frac{x_1}{1-x_1} \frac{m_W^2}{m_W^2 + Q^2} d_v(x_1, Q^2), \quad (8)$$

where G is the Fermi coupling constant, E is the energy of the incoming ν , m_W is the W -boson mass and $x_1 \equiv x/y = Q^2/2(k \cdot p_\nu)$ is the Bjorken variable associated with a nucleon bound in a nucleus. In eq.(7), d_v is the d -quark distribution inside a proton or a neutron, $D_{uu \rightarrow \pi}$ and $D_{ud \rightarrow \pi}$ are the fragmentation functions of uu or ud diquarks into positive or negative pions, $p_{1t} = p_t - (z/y)k_t$ is the transverse momentum of a pion produced on a nucleon carrying transverse momentum k_t and $z_1 = z/y$.

According to refs. [9,10] the planar graph of fig.1 (a) corresponds to one-Reggeon exchange in the t -channel, leading to the asymptotic behavior $W_X^{\alpha_R(0)-1}$, where W_X is the squared invariant mass of the undetected debris and $\alpha_R(0) = 1/2$ is the Reggeon intercept. Hence, from

$$W_X = (k+q)^2 = k^2 + Q^2 \frac{(1-\tilde{x}_1)}{\tilde{x}_1}, \quad (9)$$

where $\tilde{x}_1 = Q^2/2(k \cdot q)$, it follows that the Regge behavior of the planar graph of fig.1 (a) at moderate and large Q^2 is given by

$$W_X^{-1/2} \sim \sqrt{\frac{(1-\tilde{x}_1)}{\tilde{x}_1 Q^2}}. \quad (10)$$

The fact that the Q^2 -dependence of the graph of fig. 1 (a) is determined mainly by this Regge asymptotic is a consequence of the weak Q^2 -dependence exhibited by the calculated F_P^N .

The second contribution to the spectrum, coming from the cylindrical graph of fig. 1 (b) can also be obtained within the approach of ref. [10]. According to I, it can be written the form

$$F_C^N(x_1, Q^2; z_1, p_{1t}) = z_1 \phi_2(Q^2) \left[L_1(x_1, Q^2; z_1, p_{1t}) + \tilde{L}_1(x_1, Q^2; z_1, p_{1t}) \right. \\ \left. + L_2(x_1, Q^2; z_1, p_{1t}) + \tilde{L}_2(x_1, Q^2; z_1, p_{1t}) \right], \quad (11)$$

with

$$\phi_2(Q^2) = mE \frac{G^2}{\pi} \frac{m_W^2}{Q^2 + m_W^2}, \quad (12)$$

$$L_1 = \int_{z_1}^{1-x_1} \frac{dy}{y} \int d^2k_t \left[u_v(y, k_t; Q^2) D_{u \rightarrow \pi} \left(\frac{z_1}{y}, p_{1t} - \frac{z_1}{y} k_t \right) \right. \\ \left. d_v(y, k_t; Q^2) D_{d \rightarrow \pi} \left(\frac{z_1}{y}, p_{1t} - \frac{z_1}{y} k_t \right) \right], \quad (13)$$

$$L_2 = \int_{z_1}^{1-x_1} \frac{dy}{y} \int d^2k_t \left[\frac{4}{3} f_{ud}(y, k_t; Q^2) D_{ud \rightarrow \pi} \left(\frac{z_1}{y}, p_{1t} - \frac{z_1}{y} k_t \right) \right. \\ \left. + \frac{1}{3} \left(f_{uu}(y, k_t; Q^2) D_{uu \rightarrow \pi} \left(\frac{z_1}{y}, p_{1t} - \frac{z_1}{y} k_t \right) \right. \right. \\ \left. \left. + f_{dd}(y, k_t; Q^2) D_{dd \rightarrow \pi} \left(\frac{z_1}{y}, p_{1t} - \frac{z_1}{y} k_t \right) \right) \right], \quad (14)$$

$$\tilde{L}_1 = d_s(x_1, Q^2) D_{u \rightarrow \pi}(z_1, p_{1t}) \quad (15)$$

and

$$\tilde{L}_2 = \int_{z_1}^{1-x_1} \frac{dy}{y} \int d^2k_t \bar{d}_s(y, k_t; Q^2) D_{\bar{d} \rightarrow \pi} \left(\frac{z_1}{y}, p_{1t} - \frac{z_1}{y} k_t \right). \quad (16)$$

In the above equations u_v is the distribution of the valence u -quark, f_{uu} , f_{ud} and f_{dd} are the distributions of uu -, ud - and dd -diquarks inside the nucleon, $D_{u \rightarrow \pi}$, $D_{d \rightarrow \pi}$ are the fragmentation functions of the u - and d -quark into a pion and $D_{dd \rightarrow \pi}$ is the fragmentation function of the dd -diquark dd into a pion. The explicit expression of the quark and diquark distributions and fragmentation functions, obtained within the approach of ref. [10], are given in I.

According to refs. [9,10] the diquark distribution $f_{qq}(y)$ coincides with the distribution of the corresponding valence quark evaluated at $1-y$, i.e. with $q_v(1-y)$, if $q_v(y)$ is normalized to unity. The main contribution to the pion spectrum is coming from target fragmentation, i.e. the kinematical region corresponding to large values of $z_1 = z/y$. Within the approaches of refs. [9,10] and [11,12] the main contribution of sea quarks to the hadron spectrum is associated with n -Pomeron exchange processes (with $n \geq 2$), which are not taken into account in this analysis as they provide a vanishingly small contribution at large y [10–12]. We only include sea quarks produced from gluon decay, as shown in fig. 1 (b). In our

approach the gluon is seen as a nucleon constituent, in addition to the three valence quarks. Therefore, we have used an average value of the gluon fraction $\langle y_g \rangle$ and normalized the valence quark distribution in a nucleon to $1 - \langle y_g \rangle$, the value $\langle y_g \rangle \simeq 0.15 - 0.2$ being taken from ref. [20]. This procedure amounts to setting $f_{qq}(y) = q_v(1 - \langle y_g \rangle - y)$. Our calculations show that the contribution of fragmentation of sea quarks and antiquarks (see the cylindrical graph of fig. 1 (b)), described by the terms \tilde{L}_1 and \tilde{L}_2 , is much smaller than that coming from fragmentation of valence quarks and diquarks, described by the terms L_1 and L_2 of eq.(11).

We assume a factorized form, similar to that of eq.(5), for the quark and diquark distributions and fragmentation functions. The k_t dependence of the quark distribution is again chosen of the Gaussian form

$$g_q(k_t) = \frac{1}{\langle k_{qt}^2 \rangle \pi} e^{-k_t^2 / \langle k_{qt}^2 \rangle} , \quad (17)$$

where $\langle k_{qt}^2 \rangle$ is the average value of the squared quark transverse momentum. For the fragmentation function we have used

$$g_{q(qq) \rightarrow h}(k_t) = \frac{\gamma}{\pi} e^{-\gamma k_t^2} . \quad (18)$$

The cylindrical graph of fig. 1 (b) corresponds to one-Pomeron exchange in the t -channel, whose asymptotic behavior is $W_X^{\tilde{\alpha}_P(0)-1}$, where for the supercritical Pomeron [9,10] the value of the exponent is given by $\Delta \equiv \tilde{\alpha}_P(0) - 1 \simeq 0.1 - 0.15$ [18,19]. Hence, the Pomeron asymptotic of the cylindrical graph of fig. 1 (b) turns out to be $(k^2 + Q^2(1 - \tilde{x}_1)/\tilde{x}_1)^\Delta$. The Q^2 -dependence of the cylindrical graph is dominated by the supercritical Pomeron behavior, as F_C^N of eq.(11) depends weakly upon Q^2 .

In conclusion, the relativistic invariant spectrum of pions produced in $\nu + N \rightarrow \mu + \pi + X$ processes can be written in the form

$$\begin{aligned} \rho_{\nu N \rightarrow \mu \pi X} \equiv \frac{z d^3 \sigma}{dx_1 dz_1 dp_{1t}} &= F_P^N(x_1, Q^2; z_1, p_{1t}) \left(\frac{(k^2 + Q^2(1 - \tilde{x}_1)/\tilde{x}_1)}{s_0} \right)^{-1/2} \\ &+ F_C^N(x_1, Q^2; z_1, p_{1t}) \left(\frac{(k^2 + Q^2(1 - \tilde{x}_1)/\tilde{x}_1)}{s_0} \right)^\Delta , \end{aligned} \quad (19)$$

where $s_0 = 1 \text{ (GeV/c)}^2$ is a parameter usually introduced in Regge theory in order to get the correct dimensions. Substituting $\rho_{\nu N \rightarrow \mu \pi X}$ of eq.(19) and the nucleon distribution $f_A(y, k_t)$ into eq.(2) one can calculate the relativistic invariant spectrum of pions produced in the reaction $\nu + A \rightarrow \mu + \pi + X$.

The multiplicity of pions normalized to the cross section of the process $\nu + A \rightarrow \mu + X$, σ , defined as

$$\langle \tilde{n}_\pi \rangle \equiv \frac{\langle n_\pi \rangle}{\sigma} = \frac{1}{\sigma} \int_{x_{min}}^{x_{max}} dx \int_{z_{min}}^{z_{max}} \frac{dz}{z} \int_0^{p_{\pi max}} d^2 p_{\pi t} \rho_{\nu A \rightarrow \mu \pi X} , \quad (20)$$

can also be split into two parts, corresponding to the planar, or one-Reggeon exchange, diagram (fig. 1 (a)) and cylindrical, or one-Pomeron exchange diagram (fig. 1 (b)). While at fixed \tilde{x}_1 the first term decreases as Q^2 increases, the second increases with a slope dictated by the value of Δ . The Q^2 -dependence of $\langle \tilde{n}_\pi \rangle$ resulting from our approach is shown in fig. 2, together with experimental data taken from ref. [3].

The NOMAD collaboration carried out a study of inelastic ν - C interactions in which the negative pions emitted in the whole backward hemisphere, with respect to the incoming neutrino beam, were detected [3]. The data of fig. 2 show the multiplicity of negative pions carrying momenta in the range $0.35 < p_\pi < 0.8 \text{ GeV/c}$, measured in a kinematical setup in which W_X increases as Q^2 increases. Theoretical calculations have been performed applying the same kinematical conditions.

The results obtained including both diagrams is represented by the solid line, while the dashed and dash-dot lines correspond to the separated contributions of the cylindrical graph of fig. 1 (b) and the planar graph of fig. 1 (a), respectively.

The planar diagram provides the main contribution at small Q^2 , while the cylindrical one dominates at $Q^2 > 10 \text{ (GeV/c)}^2$. The decrease of the planar graph contribution to $\langle \tilde{n}_\pi \rangle$ and the increase of the cylindrical graph contribution with increasing Q^2 are both consequences of the kinematical setup of ref. [3], in which increasing Q^2 leads to an increase of the squared invariant mass W_X (see eqs.(9) and (19)). It clearly appears that both diagrams have to be included to explain the observed Q^2 -dependence. The fact that the solid line

lies somewhat below the experimental data at $Q^2 > 2$ (GeV/c)² is likely to be ascribed to the contribution of secondary rescattering effects, which are not taken into account in our approach.

The dotted line has been obtained setting $P(\mathbf{k}, E) \equiv 0$ in the domain of large energy and large momentum, not covered by the nonrelativistic calculations of ref. [16]. Comparison between the solid and dotted line shows that the dominant contribution to $\langle \tilde{n}_\pi \rangle$ comes from the high momentum tail of the nucleon distribution.

Numerical calculations have been carried out using values of the average squared transverse momentum, entering eq.(6), in the range $\langle k_t^2 \rangle = 0.12 - 0.14$ (GeV/c)². These values correspond to an average nucleon momentum ~ 0.4 GeV/c, which seems to be reasonable for processes dominated by the high momentum tail of the nucleon distribution. The associated ambiguity in the results is always within the experimental errors.

The other two parameters entering our calculations are the average quark and diquark transverse momentum and the slope of the Gaussian describing the k_t -dependence of the fragmentation functions. Their values have been taken from ref. [21], where a modified QGSM, explicitly including the transverse motion of quarks and diquarks, has been developed.

Besides the Q^2 dependence of the negative pion multiplicity, the NOMAD collaboration measured the semi-inclusive spectrum of negative pions, defined as

$$\frac{2\pi}{\sigma} E_\pi \frac{d\sigma}{d^3p_\pi} \equiv \frac{1}{\sigma} \frac{E_\pi}{p_\pi} \frac{d\sigma}{dp_\pi^2}, \quad (21)$$

in the kinematical region corresponding to pions emitted in the backward hemisphere with $p_\pi^2 > 0.05$ (GeV/c)² [3]. In fig. 3 we compare the p_π^2 -dependence of the experimental spectrum to that resulting from our approach. It clearly appears that the contribution of the cylindrical graph dominates the spectrum and that the inclusion of the high momentum tail of the nucleon distribution, corresponding to $p > 0.4$ GeV/c, is needed to describe the data.

In this paper we have analyzed inelastic neutrino-nucleus processes in which negative

pions are emitted in the backward hemisphere. The main conclusions of our work, concerning both the reaction mechanism and role of nuclear structure, can be summarized as follows. The dominant contribution to the reaction comes from target fragmentation, as shown by the calculation of the two topological graphs of fig. 1 within the dual topological unitarization scheme. Two kinds of the elementary processes have to be included: neutrino scattering off valence quarks, corresponding to one-Reggeon exchange in the t -channel (planar graph, fig. 1 (a)), and neutrino scattering off sea quarks, corresponding to one-Pomeron exchange in the t -channel (cylindrical graph, fig. 1 (b)). In the kinematical setup of ref. [3] the contribution of the planar graph to the analyzed pion multiplicity decreases as $\sqrt{1/Q^2}$ as Q^2 and W_X increase, while the contribution of the cylindrical graph increases as $Q^{2\Delta}$, with Δ in the range $0.1 - 0.15$, as Q^2 and W_X increase. The resulting Q^2 -dependence of the normalized multiplicity of pions emitted in the backward hemisphere in the reaction $\nu + C \rightarrow \mu^- + \pi^- + X$, turns out to be in fair agreement with the experimental data of ref. [3]. As for the role of nuclear structure, the dominant contribution is coming from the high momentum tail of nucleon distribution, which can be described in terms of overlaps of distributions of three-quark colorless objects [6]. Including both graphs of fig. 1, our approach also provides a satisfactory description of the p^2 -dependence of the measured pion spectrum.

We are indebted to A.B.Kaidalov and M.Veltri for many helpful discussions. This work was partly supported by the U.S. Department of Energy.

REFERENCES

[†] Supported by the Russian Foundation for Fundamental Research under grant 99-02-17727.

- [1] P.V. Degtyarenko *et al*, Phys. Rev. C **50**, R541 (1994).
- [2] BEBC WA 59 Collaboration. E. Matsinos *et al*, Zeit. Phys. C **44**, 79 (1989).
- [3] NOMAD Collaboration. P. Astier *et al*, Nucl. Phys. **B609**, 255 (2001).
- [4] C.E. Carlson, K.E. Lassila and U.P. Sukhatme, Phys. Lett. **B263**, 277 (1991).
- [5] G.D. Bosveld, A.E.I. Dieperink and A.G.Tenner, Phys.Rev. C **49**, 2379 (1993).
- [6] O. Benhar, S. Fantoni, G.I. Lykasov and N.V. Slavin, Phys. Rev C **55**, 244 (1997).
- [7] O. Benhar, S. Fantoni, G.I. Lykasov and N.V. Slavin, Phys. Lett. **B415**, 311 (1997).
- [8] O. Benhar, S. Fantoni and G.I.Lykasov, Eur. Phys. J. A **7**, 415 (2000).
- [9] A.B. Kaidalov, Sov. J. Nucl. Phys. **33**, 733 (1981).
- [10] A.B.Kaidalov, Phys. Lett. **B116**, 459 (1982); Sov. J. Nucl. Phys. **33**, 733 (1981); *ibidem* **45**, 902 (1987).
- [11] A. Capella, U. Sukhatme, Chung-I Tan and J. Tran Thanh Van, Phys. Lett. **B81**, 68 (1979); Z. Phys. **63**,329 (1979)
- [12] A. Capella, U. Sukhatme, Chung-I Tan and J. Tran Thanh Van, Phys. Rep. **236**, 223 (1994).
- [13] L.L. Frankfurt and M.I.Strikman, Phys. Rep. **160**, 236 (1988).
- [14] N.S. Amelin and G.I. Lykasov, Sov. J. Nucl. Phys. **33**, 100 (1981).
- [15] L.L. Frankfurt and M.I. Strikman, Phys. Rep. **76**, 215 (1981).
- [16] O. Benhar, A. Fabrocini and S. Fantoni, Nucl. Phys. **A505**, 267 (1989).

- [17] O. Benhar, S. Fantoni, G.I. Lykasov and N.V. Slavin, Phys. Rev C **57**, 1532 (1998).
- [18] A. Capella, A. Kaidalov, C. Merino and J. Tran Thanh Van, Phys. Lett. **B337**, 358 (1994); *ibidem* **B343**, 403 (1995).
- [19] A. Capella, E.G. Ferreira, C.A. Salgado and A.B. Kaidalov, Phys.Rev. D **63**, 054010 (2001).
- [20] NM Collaboration, M. Arneodo *et al*, Phys. Lett. **B309**, 222 (1993).
- [21] G.I. Lykasov and M.N. Sergeenko, Z. Phys. C **52**, 635 (1991); *ibidem* **56**, 697 (1992); *ibidem* **70**, 455 (1996).

FIGURES

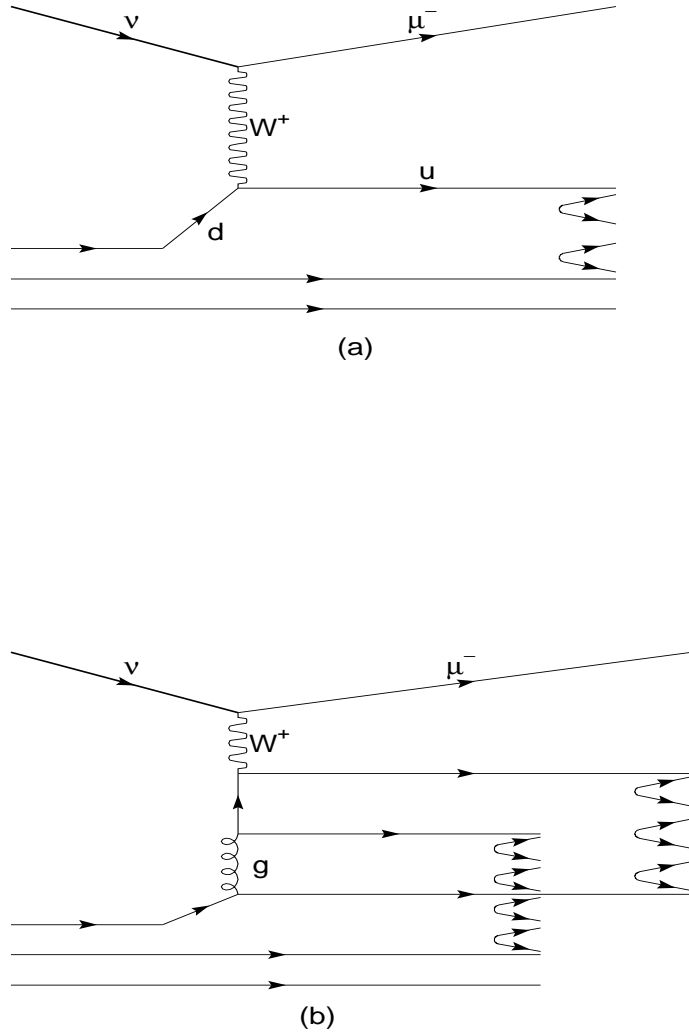


FIG. 1. Planar (a) and cylindrical (b) graphs contributing to the reaction $\nu + A \rightarrow \mu + h + X$. Diagrams (a) and (b) describe processes in which the incoming neutrino interacts with a valence quark or a sea $q\bar{q}$ pair, respectively.

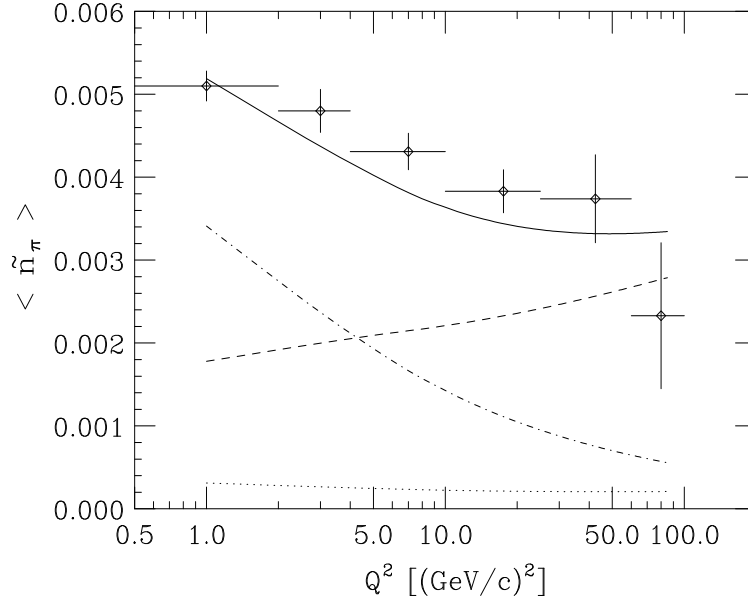


FIG. 2. Q^2 -dependence of the normalized multiplicity of pions produced in the backward hemisphere in the $\nu + C \rightarrow \mu^- + \pi^- + X$ reaction. The solid line shows the results of the full calculation, including both graphs of fig. 1. The dashed and dash-dot lines correspond to the separated contributions of the cylindrical graph of fig. 1 (b) and the planar graph of fig. 1 (a), respectively. The dots show the results obtained setting $P(\mathbf{k}, E) \equiv 0$ in the high energy-momentum domain, not covered by the nonrelativistic calculation of ref. [16]. The experimental data are taken from ref. [3].

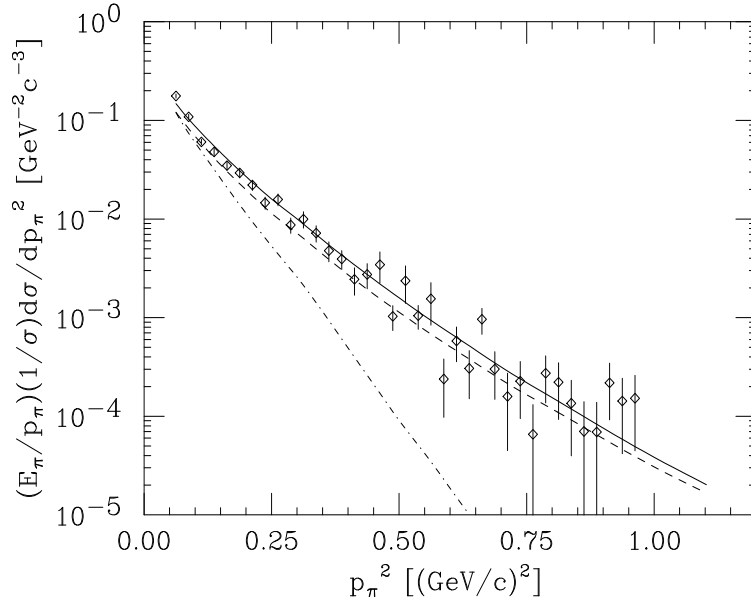


FIG. 3. p^2 -dependence of the spectrum of backward pions produced in the reaction $\nu + C \rightarrow \mu^- + \pi^- + X$. The solid curve corresponds to the full calculation whereas the dashed line has been obtained including the cylindrical graph of fig. 1 (b) only. The dash-dot line shows the results obtained setting $P(\mathbf{k}, E) \equiv 0$ in the high energy-momentum domain, not covered by the nonrelativistic calculation of ref. [16]. The experimental data are taken from ref. [3].